Detailed study on phase transitions in the dissipative anisotropic Dicke model

Pragna Das [1,2,*] and Saptarshi Saha [3,4,†]

[1] *Indian Institute of Science Education and Research Bhopal, Bhopal, Madhya Pradesh 462066, India*

[2] *Department of Theoretical Physics, J. Stefan Institute, 1000 Ljubljana, Slovenia*

[3] *Department of Physical Sciences, Indian Institute of Science Education and Research Kolkata, Kolkata, West Bengal 741246, India*

[4] *Institut für Physik und Astronomie, Technische Universität Berlin, Hardenbergstraße 36, 10623 Berlin, Germany*

(Received 22 January 2026; accepted 8 July 2026; published 31 July 2026)

We present a comprehensive study of different phase transitions in the Dicke model incorporating both anisotropy and dissipation. We begin with a concise review of the quantum phase transition in this setting, highlighting how these two parameters shift the critical point. We then perform a detailed investigation of the transition from ergodic to nonergodic phases by analyzing the eigenvalue and eigenvector properties of the Liouvillian with the aid of scaling of the Liouvillian gap and the average participation ratio. Our results show that the eigenvector properties of the Liouvillian are consistent with its spectral characteristics, leading to a phase diagram that has similarities to the closed counterpart. In particular, the steady-state properties are associated with the quantum phase transition, whereas the decaying modes retain signatures of the ergodic to nonergodic transition. Furthermore, we demonstrate that the Liouvillian gap exhibits distinct scaling behaviors in these two phases. Finally, we extend our study to the driven case by applying a Thue-Morse quasiperiodic drive. In this case, we find that bosonic dissipation plays a crucial role in stabilizing the prethermal plateau, offering an effective mechanism to halt the heating effect arising from the quasiperiodic drive.

DOI: 10.1103/47gn-l4dm

I. INTRODUCTION

Exploring many-body quantum dynamics through atom-photon interaction is the heart of atomic, condensed-matter, and ultracold quantum physics [1–4]. Experiments using the cavity QED setup provide an ideal platform to investigate the underlying microscopic properties, e.g., the collective effects, various phase transitions, and Bose-Einstein condensation [5–8]. From a theoretical perspective, the Dicke model is an iconic model for understanding the above aspects of such systems [9–11].

The study of collective light-matter interactions traces back to the pioneering work of Dicke, which describes the interaction between an ensemble of N atoms with a single-mode bosonic field via a dipolar coupling strength [12–15]. In the thermodynamic limit $N \to \infty$, the model shows a quantum phase transition (QPT) from the normal phase to the superradiant phase [10,12,16–19]. Along with it, such a model also shows the excited-state quantum phase transition and thermal phase transition under different circumstances. The first experimental proposal of observing the Dicke quantum phase transition using multilevel atoms and cavity-mediated Raman transitions was proposed by Dimer *et al.* [8]. Around the same time, Baumann *et al.* observed the Dicke phase transition in an open system consisting of a Bose-Einstein condensate coupled to an optical cavity, highlighting the emergence of a self-organized supersolid phase [20]. Such studies were later extended to observe Higgs and Goldstone modes in a supersolid quantum gas [2].

A dissipative realization of the generalized Dicke model was also introduced to observe the effects from the counterrotating terms, and the effect of an external drive was further explored [21]. The generalized version of the Dicke model, as mentioned above, namely, the anisotropic Dicke model (ADM) [21–25], where the coupling strengths correspond to the rotating and counterrotating terms, is considered to be different. Due to the asymmetry in the coupling strengths, the ADM shows novel features in addition to the well-known existing properties, i.e., the ergodic to nonergodic transition (ENET) [22,26]. There exists a one-to-one correspondence between the nonergodic phase and the integrability of the system. Hence, a detailed study on the nonergodic phase will be useful in understanding the following emerging phenomena, e.g., many-body localization, quantum scars, and prethermalization [27–29]. On the other hand, the ergodic phase connects to the nonintegrable phase, a path to study the quantum chaos [30,31]. A natural question therefore concerns how the aforementioned phases behave in the presence of dissipation and in particular whether dissipation destroys their nonergodic character.

In most cases, a leaky cavity is considered to introduce dissipative effects in the atom-photon interaction [10,17,32,33]. In the case of the QPT, the effect of dissipation was

*Contact author: pragnad90@gmail.com

†Contact author: s.saha@tu-berlin.de

Published by the American Physical Society under the terms of the Creative Commons Attribution 4.0 International license. Further distribution of this work must maintain attribution to the author(s) and the published article's title, journal citation, and DOI.

previously explored [17]. It is worth studying the impact of dissipation in the ENET, which we explore in this paper. The Hamiltonian approach is insufficient to capture such dissipative dynamics. Hence, we adapt the Liouvillian approach motivated by the Lindblad quantum master equation to incorporate the nonunitary dynamics [34]. In this prescription, the Liouvillian gap Δ plays an important role in characterizing the asymptotic convergence to the steady state [35–52]. The dependence of such a Liouvillian gap on the system size for various systems has already been studied, where the nature of the dissipation and the corresponding phases determine such a scaling [36,37,41,46,47]. Based on these results, one can conjecture that the length dependence of the Liouvillian gap is also sensitive to the specific phases of many-body dissipative systems. Motivated by this perspective, we aim to investigate the system-size dependence of the Liouvillian gap for the ENET in the ADM. Similarly, the level statistics of the eigenvalues of the Liouvillian provide useful information regarding the phases. For example, in the case of the ADM, the system follows the two-dimensional Poisson statistics in the nonergodic phase, whereas in the ergodic phase the system behaves as the Ginibre ensemble [53–57]. For completeness of the above analysis, the distribution of the eigenvector is further required. We note that for non-Hermitian systems, the correspondence between the eigenvalue-eigenvector property is quite different from its Hermitian counterpart. Motivated by this fact, we performed the study of the average participation ratio of the dissipative ADM to provide further explanation for the emergence of the ENET.

Another important aspect of a many-body quantum system is exploring the dynamics under an external drive [58]. In such cases, it is expected that the system will reach the infinite temperature state (e.g., thermal state) [59,60]. An essential distinction can be observed for the periodic drive, where instead of thermalization a prethermal quasisteady state emerges in the intermediate timescale [61–64]. Using the Floquet theory, an effective Hamiltonian can be constructed for the prethermal state in the high-frequency limit, and the relevant conserved quantities can be derived subsequently [65]. More recently, research interest has shifted towards exploring quantum dynamics under a quasiperiodic drive [64,66–71], where it is expected that the lifetime of the prethermal phase is shortened due to the absence of temporal order. As such, the quasiperiodic drive further pushes it to the thermal state. A similar study was also reported in our previous work of the ADM [64]. A further question concerns what happens in the presence of dissipation. We want to specify the reason why such a study is important. In the case of the dissipative ADM, we consider the spontaneous emission of the cavity modes. Therefore, the cavity and the atoms try to reach their respective ground state in the presence of strong dissipation. The ground state has the lowest entanglement entropy (EE). At the same point, the quasiperiodic drive increases the EE due to heating. We expect a competition between the strength of the quasiperiodic drive and the dissipation rate in this system. We mostly focus on whether the strong dissipation stabilizes the prethermal phase or the quasiperiodic drive dominates the heating process. We also show that such a mechanism is different for the ergodic and nonergodic phases.

As stated above, the primary motivation of this paper is to investigate the impact of dissipation on the emergent phases of the ADM in both undriven and driven scenarios. To this end, we outline the structure and main results of the paper as follows. In Sec. II we introduce the dissipative ADM, where a spin-boson system is coupled to an additional bosonic environment. We begin with the undriven case in Sec. III. The existence of a QPT is analyzed in Sec. III A, followed by a detailed study of the ENET in Sec. III B. In particular, we examine the Liouvillian gap in Sec. III B 1 and investigate the properties of the corresponding eigenvectors in Sec. III B 2. We then turn to the driven case in Sec. IV, where the quasiperiodic driving protocol is defined in Sec. IV A and the role of dissipation in the presence of drive is discussed in Sec. IV B. Finally, we summarize our findings and present a broader perspective on their implications in Sec. V. Throughout the paper, we adopt the following notation: Operators in Hilbert space are denoted by $\hat{\mathcal{O}}$, eigenvectors in Hilbert space are denoted by $|\psi\rangle$, superoperators in Liouville space are denoted by $\hat{\hat{\mathcal{O}}}$, and eigenvectors of the superoperator in Liouville space are denoted by $|\hat{\rho}\rangle$.

II. DESCRIPTION OF THE SYSTEM

Here we consider a system consisting of N noninteracting two-level atoms coupled with a single-mode bosonic leaky cavity. The corresponding Hamiltonian of the system is

$$\hat{\mathcal{H}} = \omega a^\dagger a + \omega_0 J_z + \frac{g_1}{\sqrt{N}}(a^\dagger J_- + a J_+) + \frac{g_2}{\sqrt{N}}(a^\dagger J_+ + a J_-), \tag{1}$$

where g_1 and g_2 are the corresponding rotating and counterrotating spin-boson coupling strengths. In general, $g_1 \neq g_2$ indicates the anisotropy in the Dicke model [25], and $g_1 = g_2 = g$ recovers the original isotropic Dicke model. Here a ($a^\dagger$) is the bosonic annihilation (creation) operator, $J_\alpha = \sum_{i=1}^{N} \frac{1}{2}\sigma_\alpha^i$ ($\alpha = x, y\ z$) is total angular momentum of the ensemble of N atoms, ω is the bosonic mode frequency, and ω_0 is the level splitting of the atoms. The first two terms represent the free Hamiltonian of the bosonic cavity and atoms, respectively. The basis of the Hamiltonian is $|n, m\rangle$, where $n = 0, 1, 2, \ldots, n_{\max}$ is the boson number and for the symmetric spin subspace considering even J, $m = -J, -J+1, \ldots, 0, \ldots, J-1, J$. Thus, the Hilbert space dimension of the closed system is $N_{\mathrm{D}} = (N+1)(n_{\max}+1)$.

We assume that the spontaneous emission rate of the leaky cavity is κ and all other sources of dissipation and dephasing are excluded in our model. The dynamics can be explained by the Lindblad master equation in the Markovian regime [34]. The dynamical equation of the density matrix of the atom plus cavity in the Liouville space is given by

$$\frac{d|\hat{\rho}\rangle}{dt} = \hat{\hat{\mathcal{L}}}|\hat{\rho}\rangle, \tag{2}$$

where $|\hat{\rho}\rangle$ is density matrix of the system in Liouville space and $\hat{\hat{\mathcal{L}}}$ is the Liouvillian superoperator. The explicit form of

$\hat{\hat{\mathcal{L}}}|\hat{\rho}\rangle$ in the Hilbert space is

$$\hat{\hat{\mathcal{L}}}|\hat{\rho}\rangle \Rightarrow -i[\hat{\mathcal{H}}, \hat{\rho}] + \kappa(2a\hat{\rho}a^{\dagger} - \{a^{\dagger}a, \hat{\rho}\}). \tag{3}$$

The corresponding analytical form of $\hat{\hat{\mathcal{L}}}$ is given by

$$\hat{\hat{\mathcal{L}}} = -i[(\hat{\mathcal{H}} \otimes \hat{\mathcal{I}}) - (\hat{\mathcal{I}} \otimes \hat{\mathcal{H}}^{T})] + \kappa(2a \otimes a^{*} - a^{\dagger}a \otimes \hat{\mathcal{I}} - \hat{\mathcal{I}} \otimes a^{\dagger}a). \tag{4}$$

The basis of the Liouvillian is $|n_l, m_l\rangle \otimes |n_r, m_r\rangle$ and the corresponding Liouvillian space dimension is $N_{\mathrm{L}} = N_{\mathrm{D}} \times N_{\mathrm{D}}$. Using parity symmetry, the dimension of the Liouvillian space is reduced to $\frac{N_{\mathrm{L}}}{2}$ [72]. In such systems, we are primarily interested in the following phases: (i) the absence of an external drive, including (a) normal and superradiant phases and (b) ergodic and nonergodic phases, and (ii) the presence of an external drive, including the prethermal phase and further heating.

In the remainder of the paper we will briefly discuss the existence of such phases in the ADM.

III. ANALYSIS OF THE UNDRIVEN CASE

We begin with the undriven case, where we aim to study the effects of dissipation on the QPT and ENET.

A. Emergence of the quantum phase transition

As the QPT is well defined and has been discussed thoroughly in previous works, we provide a concise review of this phenomenon. Let us consider an isotropic Dicke model $g_1 = g_2$. The Hamiltonian of the system is invariant under the transformations $a \to -a$ and $\sigma_x \to -\sigma_x$ (i.e., $\mathbb{Z}_2$ symmetry). The QPT is defined in this case as the breaking of $\mathbb{Z}_2$ symmetry. As such, the normal phase is the $\mathbb{Z}_2$ protected phase, with $\langle a \rangle = 0$, and in the case of a symmetry-broken superradiant phase, $\langle a \rangle \neq 0$ [10]. Following the retarded Green's function and the Keldysh path-integral formalism, the critical coupling strength for the second-order QPT is defined as $g_c = \frac{1}{2}\sqrt{\omega\omega_0}\sqrt{1 + \kappa^2/\omega^2}$. Following the same procedure, in the case of the ADM, instead of a line, we get a region of g_1 and g_2, which satisfies the relation

$$\left(g_1^2 - g_2^2\right)^2 - 2\left(g_1^2 + g_2^2\right)\omega\omega_0 + (\omega^2 + \kappa^2)\omega_0^2 = 0. \tag{5}$$

Several experimental platforms have been developed to observe the QPT in the Dicke model [2,8,20].

B. Emergence of the ergodic to nonergodic phase transition

In this section we provide a concise review of the ENET in the closed ADM. In the case of the ADM, the system is integrable for $g_1 = 0$ or $g_2 = 0$. As a consequence, the system shows the ENET in the vicinity of the integrable regime. Previous work shows the emergence of the ENET in the closed ADM with the aid of a level-spacing ratio and also shows that such a phase transition is not the precursor of the QPT [22]. We will further extend this approach to the dissipative case and study the properties of the Liouvillian of such systems for different values of g_1 and g_2.

1. Finite-size scaling of the Liouvillian gap

An analysis using the eigenvalues of the Liouvillian $\hat{\hat{\mathcal{L}}}$ is required to understand the ENET in the ADM. The real part of the eigenvalues of $\hat{\hat{\mathcal{L}}}$ is always less than or equal to zero. The real zero eigenvalue shows the notion of the steady state. On the other hand, the negative real parts are the decaying modes. If the complex part is nonzero, then such eigenmodes show oscillatory behavior [38,73]. Whether such oscillation is long lived or not is decided by the corresponding real part of the eigenvalue. The Liouvillian gap Δ is defined by the real distance of the nearest-neighbor eigenvalue of $\hat{\hat{\mathcal{L}}}$ from its zero eigenvalue

$$\Delta = \min[\mathrm{Re}(E_0 - E_n)], \tag{6}$$

where E_n are the eigenvalues of the Liouvillian and $E_0 = 0 + 0i$ is the corresponding minimum eigenvalue. The inverse of the Liouvillian gap, $1/\Delta$, shows the notion of the relaxation time of the system. In Fig. 1(a) we plot $\ln \Delta$ versus $\ln N$ for fixed $g_1 = 1.0$ and $\kappa = 0.1$ and different values of g_2 ($0.1 \leqslant g_2 \leqslant 1.5$). From the linear fits in Fig. 1(a), we extract the scaling exponent z defined by $\Delta \propto N^z$. The resulting dependence of z on g_2 is shown in Fig. 1(b). We find that the slope of z is different for the nonergodic phase and the ergodic phase. The system exhibits a nonergodic response when g_2 is small, while increasing g_2, we find a crossover into the ergodic phase. A more thorough analysis is required to reliably identify the phase boundary of the ENET, in a manner similar to that used for characterizing a QPT.

A true phase transition would require taking the thermodynamic limit $N \to \infty$; however, the high dimensionality of the system makes this limit challenging to access. Hence, our result shows a phase crossover between the ergodic and nonergodic phases rather than a phase transition. We check the same for $g_1 = 1.0, 1.25$ and $\kappa = 0.1, 0.01$ in Fig. 1(b), and our result shows that for changing κ, the system shows a qualitatively similar response. We also provide a contour plot of the exponent z by varying g_1 and g_2 in Appendix B to provide other details on the ENET.

2. Average participation ratio using eigenvector properties

The eigenvalue properties of the Liouvillian for the dissipative Dicke model have been thoroughly studied previously [72]. A recent study including the anisotropic case of this particular model also exists [74]. However, for completeness, a study requires both the eigenvalue and the eigenvector properties to understand the phase diagram of this model. We also note that for non-Hermitian systems, the correspondence between the eigenvalue and eigenvector is not as straightforward as in the Hermitian case. For example, if the Liouvillian of the dissipative system has a nonzero real eigenvalue, then the corresponding eigenvector is traceless, which is not true for the Hamiltonian of the Hermitian case. This observation motivates us to study the eigenvector properties of the dissipative ADM in order to gain deeper insight into the ENET.

In general, the Liouvillian is a non-Hermitian matrix with complex eigenvalues $\hat{\hat{\mathcal{L}}}|\hat{\rho}_i\rangle = \lambda_i|\hat{\rho}_i\rangle$. If $\hat{\hat{\mathcal{L}}}$ is diagonalizable, then using the spectral decomposition theory, any operator $\hat{\hat{A}}$ in the Liouville space can be written as $\hat{\hat{A}} = \sum c_i|\hat{\rho}_i\rangle$. The value of c_i can be calculated from the standard orthogonality

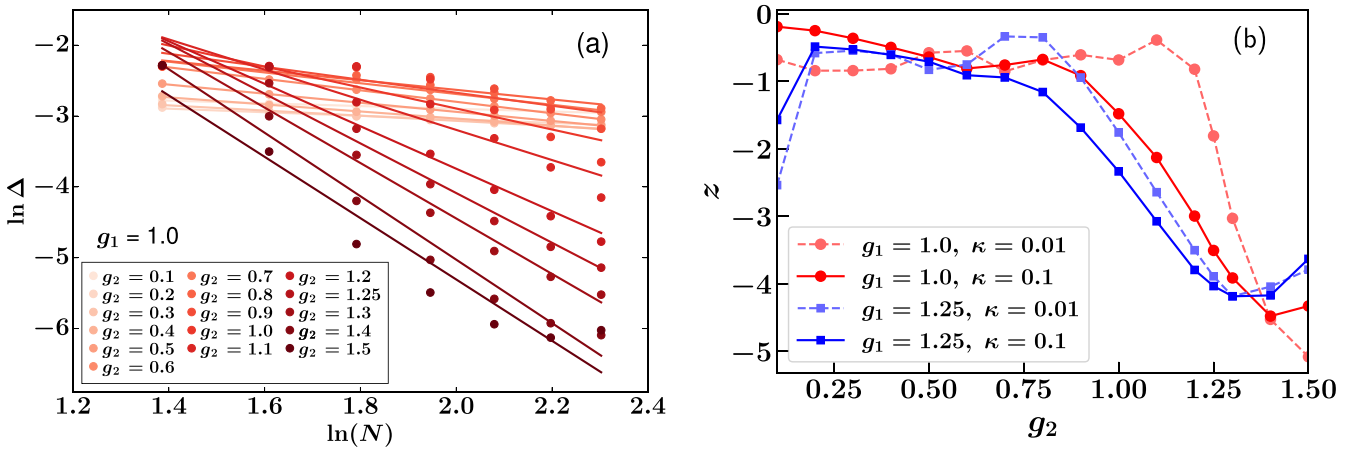


FIG. 1. (a) Plot of $\ln \Delta$ vs $\ln N$ for $g_1 = 1.0$ and $\kappa = 0.1$. (b) Slope z (extracted from the scaling of the Liouvillian gap Δ as a function of atom number) as a function of g_2 for fixed g_1 values and dissipation strengths $\kappa = 0.1$ and 0.01. Here $n_{\max} = 26$ and N varies from 4 to 10. We find that the scaling is different for the ergodic and nonergodic phases. We also show that for changing κ, the qualitative features of the ENET remain the same.

relation for a non-Hermitian matrix, $\langle\hat{\Theta}_j|\hat{\rho}_i\rangle = \delta_{ij}$. Here $\langle\hat{\Theta}_j|$ is the left eigenvector of $\hat{\hat{\mathcal{L}}}$, i.e., $\langle\hat{\Theta}_i|\hat{\hat{\mathcal{L}}} = \langle\hat{\Theta}_i|\lambda_i$ or $\hat{\hat{\mathcal{L}}}^\dagger|\hat{\Theta}_i\rangle = \lambda_i^*|\hat{\Theta}_i\rangle$. The above definition implies that to calculate the participation ratio (PR) $P \propto \frac{1}{\sum_{i=1}^{N_L/2}|c_i|^4}$ [25], we must use a biorthogonal basis consisting of both left and right eigenvectors. We note that the results corresponding only to the left and only to the right are not quite correct and may provide wrong results.

Here we perform the LU decomposition for biorthogonalization. Let $\langle\hat{L}|$ and $|\hat{R}\rangle$ be the corresponding left and right eigenvectors of $\hat{\hat{\mathcal{L}}}$ and we define $\hat{L}^\dagger\hat{R} = \hat{M}$ (here $\hat{L}^\dagger$ and $\hat{R}$ represent the operators in the Hilbert space of $\langle\hat{L}|$ and $|\hat{R}\rangle$). The matrix $\hat{M}$ can be represented in its LU-decomposed form $\hat{M} = \hat{M}_L\hat{M}_U$, where $\hat{M}_L$ ($\hat{M}_U$) is the lower (upper) triangular matrix. Hence, $\hat{L}^\dagger\hat{R} = \hat{M}_L\hat{M}_U$. Following the above approach, one can redefine the left and right eigenvectors as $\hat{L} \to \hat{L}(\hat{M}_L^{-1})^\dagger$ and $\hat{R} \to \hat{R}\hat{M}_U^{-1}$ (such that $\hat{L}^\dagger\hat{R} = \hat{\mathcal{I}}$) to make the Liouvillian space biorthogonal. The definition of the PR is given by [75]

$$P_n^{\mathrm{LR}} = \frac{\left(\sum_i |\hat{\psi}_i^n|\right)^2}{\sum_i |\hat{\psi}_i^n|^2}. \tag{7}$$

The superscript LR in P_n^{LR} denotes the biorthogonal participation ratio. The coefficients are defined as

$$\hat{\psi}_i^n = \langle\hat{L}_n|\hat{B}_i\rangle\langle\hat{B}_i|\hat{R}_n\rangle. \tag{8}$$

The set $\{|\hat{B}_i\rangle\}$ forms the Fock-space computational basis in Liouville space, i.e., $|\hat{B}_i\rangle \equiv |n_l, m_l\rangle \otimes |n_r, m_r\rangle$. Using the Hilbert-Schmidt inner product, the expressions are given by $\langle\hat{L}_n|\hat{B}_i\rangle = \mathrm{Tr}(\hat{L}_n^\dagger\hat{B}_i)$ and $\langle\hat{B}_i|\hat{R}_n\rangle = \mathrm{Tr}(\hat{B}_i^\dagger\hat{R}_n)$. Finally, the average participation ratio is defined as $P_{\mathrm{av}}^{\mathrm{LR}} = \frac{1}{N_L/2}\sum_n P_n^{\mathrm{LR}}$. We have verified that these results remain consistent even without employing the LU decomposition. In Fig. 2 we show the value of $P_{\mathrm{av}}^{\mathrm{LR}}$ as a function of the coupling strengths. In the dark portion, the average participation ratio is relatively low, which indicates the nonergodic phase, compared to the light color regime, where the average participation is quite high and represents the ergodic phase. The phase diagram is similar to Fig. 8 in Appendix A, where we show the transition from the nonergodic phase to the ergodic phase with the aid of the level-spacing ratio of eigenvalues of $\hat{\hat{\mathcal{L}}}$. Hence, we conclude that the eigenvector properties of our system are consistent with the eigenvalue properties. Our result also indicates that under small dissipation, the system is consistent with nonergodic behavior in the vicinity of $g_1 = 0$ or $g_2 = 0$. We also provide supporting plots in Appendix C to demonstrate that the qualitative features remain unchanged as the dissipation rate κ is varied.

We emphasize that the eigenstate-based analysis provides an additional perspective that is fully consistent with the information already encoded in the eigenvalue spectrum, offering an alternative and often insightful way to interpret the same

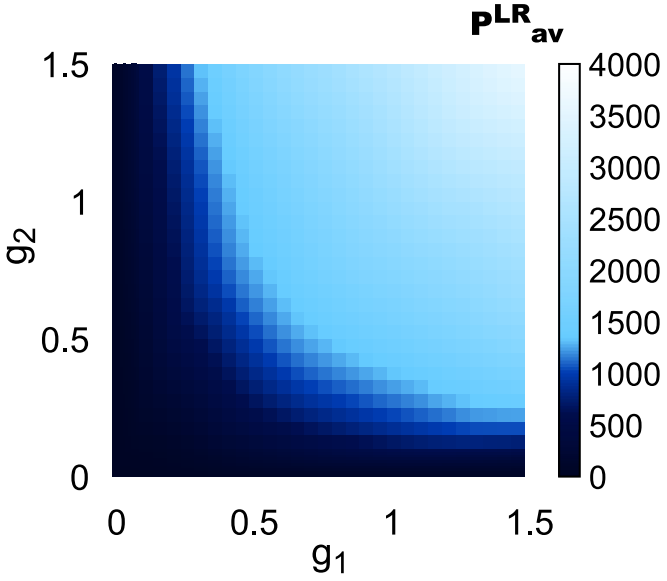


FIG. 2. Average participation ratio P_{av}, using a biorthonormal basis considering both left and right eigenvectors of the Liouvillian for the dissipative ADM as a function of the rotating and counter-rotating coupling parameters g_1 and g_2, with $N = 10$, $n_{\max} = 26$, $\omega_0 = \omega = 1$, and $\kappa = 1$.

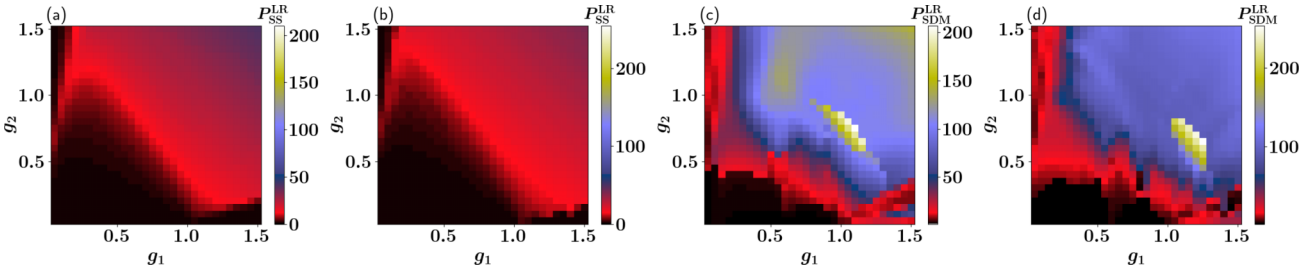


FIG. 3. Participation ratio of (a) and (b) the steady state P_{SS}^{LR} and (c) and (d) the slowest decaying mode P_{SDM}^{LR}, using the biorthonormal basis considering both left and right eigenvectors of the Liouvillian $\hat{\tilde{\mathcal{L}}}$ for the dissipative ADM as a function of the rotating and counterrotating coupling parameters g_1 and g_2. The other parameters are $N = 4$, $n_{max} = 10$, $\omega_0 = \omega = 1$, and (a) and (c) $\kappa = 0.1$ and (b) and (d) $\kappa = 0.01$. The steady-state properties exhibit clear signatures of the QPT, whereas the properties of the slowest decaying mode indicate the presence of the ENET. To facilitate a direct comparison between different parameter regimes, a common color-bar scale is used for all panels. We expect the phase transition to become progressively sharper and better resolved with increasing N and n_{max}, indicating convergence toward the thermodynamic limit.

underlying structure. Our aim is to probe a distinct aspect of the ENET, i.e., how its signatures are encoded at the level of eigenvectors. This provides a nontrivial consistency check: A robust characterization of the transition should be reflected in both eigenvalues and eigenvectors. While the eigenvalue-based approaches are technically more straightforward, they do not fully address the broader theoretical question. In particular, the structure of Liouvillian eigenvectors has not been systematically explored in prior works, which have largely focused on steady states and slow decaying modes. Our analysis therefore addresses this gap and demonstrates that the eigenvector-based approach can capture the same phenomenology, thereby reinforcing the overall understanding of the ENET in the ADM. In this context, studying the PR of the Liouvillian eigenmodes, particularly those associated with the slowest decay rates, can provide additional insight into the ENET. Since our results show that the finite-size scaling of the Liouvillian gap exhibits clear signatures of the ENET [Figs. 1(a) and 1(b)], one expects that the behavior of the PR for the slowest decaying mode should be consistent with and complementary to the conclusions drawn from the Liouvillian-gap analysis.

To support our claim, we consider a minimal model in the weak-dissipation regime. Specifically, we choose $N = 4$, $n_{max} = 10$, and $\omega, \omega_0 \gg \kappa$. Hence, for this small system size, we observe a phase crossover rather than a genuine phase transition if it exists. We investigate the behavior of the PR for both the steady state, P_{SS}^{LR}, and the slowest decaying mode, P_{SDM}^{LR}, as a function of g_1 and g_2, as shown in Figs. 3(a)–3(d). It is well known that a QPT in the closed system is associated with a phase transition of the ground state that occurs at the boundary of $|g_1 + g_2| = 1$ [25]. In the weak-dissipation regime, we find that P_{SS}^{LR} exhibits a similar signature [Figs. 3(a) and 3(b)], indicating that the QPT remains fundamentally encoded in the steady-state properties of the dissipative system.

Furthermore, in the closed ADM, the ENET is associated with a phase transition that occurs in the middle excited-state spectrum [25]. The behavior of P_{av} serves as an effective indicator of this transition, and our results for the dissipative case Fig. 2 are already consistent with those of the corresponding closed system. At the same time, motivated by the scaling of Liouvilian gap [Figs. 1(a) and 1(b)], we analyze the P_{SDM}^{LR} in Figs. 3(c) and 3(d). We demonstrate that it successfully captures the remnant signature of the ENET in the open system. Therefore, we conclude that while the QPT is primarily associated with the steady state, the ENET is linked to decaying modes in open quantum systems.

It is worth emphasizing that the decaying modes of the Liouvillian also possess fundamental physical significance. These modes encode essential dynamical properties of the system, yet their role has largely been overlooked in previous studies of driven-dissipative phases in many-body open quantum systems. Our results highlight that valuable information about nonequilibrium phase structure, particularly the presence of the ENET, can be extracted from the slowest decaying Liouvillian modes, thereby extending the conventional focus beyond steady-state properties alone.

IV. ANALYSIS OF THE DRIVEN CASE

In our earlier study of the closed version of the driven ADM [64], we showed that under the external periodic drive, the system reaches a long-lived prethermal plateau that escapes Floquet heating. In contrast, for the quasiperiodic drive, the system features a short-lived prethermal plateau, and further heating is observed. At the same time, the dynamics shows the following properties: (i) Upon increasing the drive frequency, the heating process becomes slow, and (ii) in the nonergodic regime, for the same driving frequency, heating occurs more slowly than in the ergodic regime.

Such an analysis can also be extended to the dissipative case. In the case of strong bosonic dissipation, the system will reach the ground state where the mutual information between the spins and boson is zero, whereas the quasiperiodic drive pushes the system to a state with higher mutual information. Hence, a competition between the quasiperiodic drive and the bosonic dissipation can be expected in this case.

A. Driving protocol

We briefly discuss the quasiperiodic driving protocol. In particular, we consider the quasiperiodic protocol consisting of the Thue-Morse sequence. Here we define two

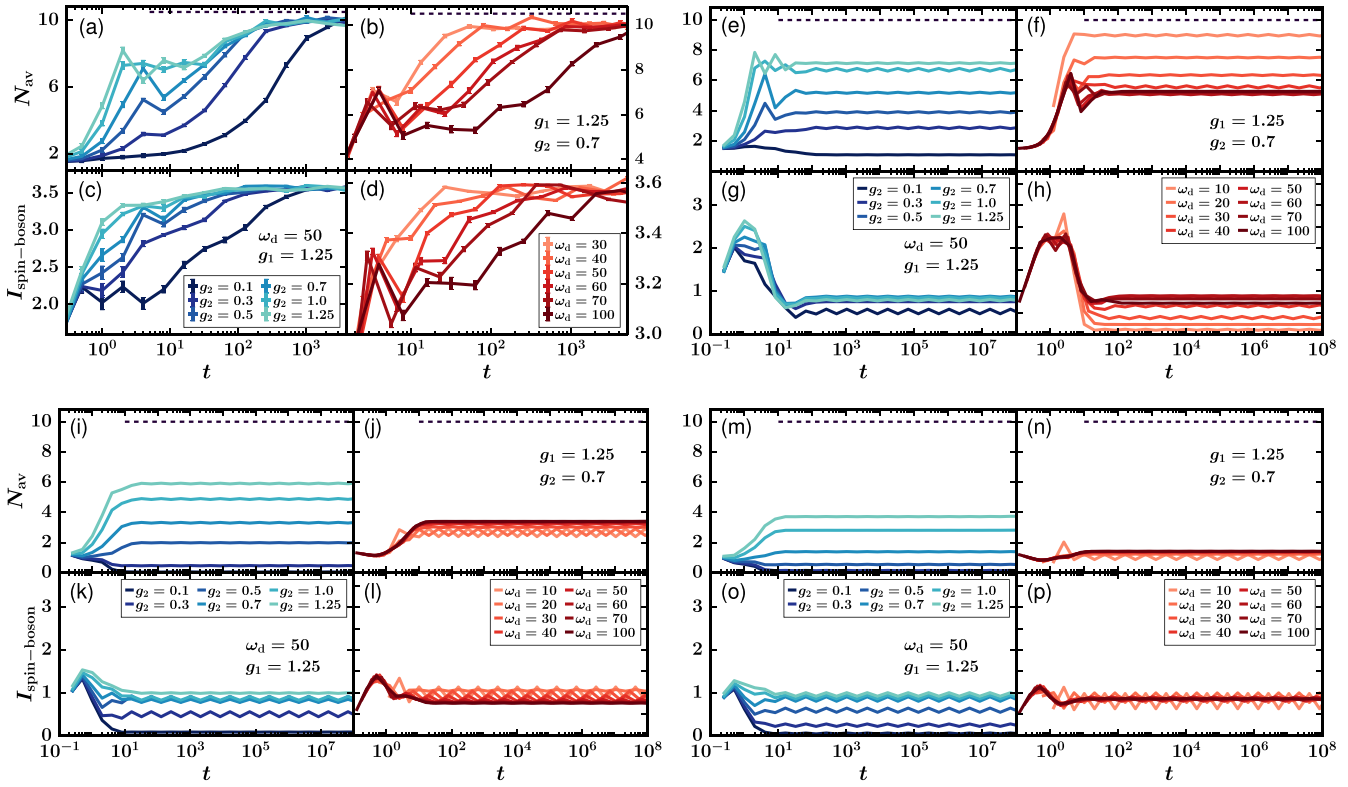


FIG. 4. (a), (b), (e), (f), (i), (j), (m), and (n) Average boson number $N_{av}(t)$ and (c), (d), (g), (h), (k), (l), (o), and (p) mutual information between spins and bosons $I_{spin\text{-}boson}$ as a function of time $t_n = 2^n T$ for the dissipative ADM under the Thue-Morse quasiperiodic drive. The initial states have low energies so that $\langle E_{in}\rangle = 0.25$. Data are shown for (a), (c), (e), (g), (i), (k), (m), and (o) a fixed driving frequency $\omega_d = 50$, $g_1 = 1.25$, and various values of g_2 and (b), (d), (f), (h), (j), (l), (n), and (p) $g_1 = 1.25$, $g_2 = 0.7$, and various values ω_d. In all panels, the driving amplitude is $\Omega = 1.0$, $N = 6$, $n_{max} = 20$, and $\omega_0 = \omega = 1$. In addition, (a)–(d) $\kappa = 0.0$, (e)–(h) $\kappa = 0.05$, (i)–(l) $\kappa = 0.6$, and (m)–(p) $\kappa = 1.0$. Time t is in units of ω_0^{-1}. The dashed line represents the page value.

Hamiltonians $\hat{\mathcal{H}}_\pm = \omega a^\dagger a + \omega_0 J_z + \frac{g_1 \pm \Omega}{\sqrt{N}}(aJ_+ + a^\dagger J_-) + \frac{g_2 \pm \Omega}{\sqrt{N}}(aJ_- + a^\dagger J_+)$, where Ω is the driving amplitude, and the corresponding Liouvillians using Eq. (4) are $\hat{\hat{\mathcal{L}}}_\pm$. The Thue-Morse sequence [66–69] can be constructed by starting with the time-evolution operators $\hat{\hat{\mathcal{U}}}_\pm = \exp(\hat{\hat{\mathcal{L}}}_\pm T)$. We can build up the next sequence using $\hat{\hat{\mathcal{U}}}_1 = \hat{\hat{\mathcal{U}}}_-\hat{\hat{\mathcal{U}}}_+$ and $\hat{\hat{\mathcal{U}}}_1 = \hat{\hat{\mathcal{U}}}_+\hat{\hat{\mathcal{U}}}_-$, $\hat{\hat{\mathcal{U}}}_2 = \hat{\hat{\mathcal{U}}}_1\hat{\hat{\mathcal{U}}}_1$ and $\hat{\hat{\mathcal{U}}}_2 = \hat{\hat{\mathcal{U}}}_1\hat{\hat{\mathcal{U}}}_1$, and so on. The driving unit cells of time length $2^n T$ can be recursively constructed as $\hat{\hat{\mathcal{U}}}_{n+1} = \hat{\hat{\mathcal{U}}}_n\hat{\hat{\mathcal{U}}}_n$ and $\hat{\hat{\mathcal{U}}}_{n+1} = \hat{\hat{\mathcal{U}}}_n\hat{\hat{\mathcal{U}}}_n$. The time evolution of the initial density matrix is given by $|\hat{\rho}_n\rangle = |\hat{\rho}(t = 2^n T)\rangle = \hat{\hat{\mathcal{U}}}_n|\hat{\rho}_{in}\rangle$, where $|\hat{\rho}_{in}\rangle = |\psi_{in}\rangle \otimes |\psi_{in}\rangle$, with $|\hat{\rho}_{in}\rangle$ the initial density matrix in the Liouville space and $|\psi_{in}\rangle$ the initial state in the Hilbert space. We also define $\omega_d = 2\pi/T$. Here we take the average over 20 low-energy eigenstates (starting from the ground state) of the decoupled Hamiltonian ($g_1 = g_2 = 0.0$).

B. Effect of tdissipation in Floquet heating

To study quantum dynamics, we define the following relevant observables: the average boson number

$$N_{av}(t) = \mathrm{Tr}[\hat{\rho}(t) \times a^\dagger a] \tag{9}$$

and the mutual information between spins and bosons

$$I_{spin\text{-}boson} = S_{spin} + S_{boson} - S_{spin\text{-}boson}, \tag{10}$$

where $S_{spin\text{-}boson} = -\mathrm{Tr}\{\hat{\rho}(t)\ln[\hat{\rho}(t)]\}$ and $S_{spin\,(boson)} = -\mathrm{Tr}\{\hat{\rho}_{spin\,(boson)}(t)\ln[\hat{\rho}_{spin\,(boson)}(t)]\}$ are the corresponding entropies and $\hat{\rho}_{spin}(t) = \mathrm{Tr}_{boson}[\hat{\rho}(t)]$ and $\hat{\rho}_{boson}(t) = \mathrm{Tr}_{spin}[\hat{\rho}(t)]$ are the corresponding reduced density matrices of the spin and boson obtained by tracing over the bosonic and spin degrees of freedom, respectively. In Fig. 4 we consider low-energy initial states subjected to the Thue-Morse driving protocol. We present the time evolution of the average boson number [Figs. 4(a), 4(b), 4(e), 4(f), 4(i), 4(j), 4(m), and 4(n)] and the mutual information between spins and bosons [Figs. 4(c), 4(d), 4(g), 4(h), 4(k), 4(l), 4(o), and 4(p)]. These quantities are shown for a fixed intermediate driving frequency ω_d and various values of the coupling parameter g_2 [Figs. 4(a), 4(c), 4(e), 4(g), 4(i), 4(k), 4(m), and 4(o)]. In addition, we analyze the same observables for a fixed (g_1, g_2) pair corresponding to the chaotic undriven model while varying the driving frequency ω_d [Figs. 4(b), 4(d), 4(f), 4(h), 4(j), 4(l), 4(n), and 4(p)].

The following are the key observations in this case.

(i) Figures 4(a)–4(d) correspond to $\kappa = 0$ and show a result similar to that for the closed quasiperiodic driven ADM.

(ii) For small values of $\kappa = 0.05$, we show that further heating is minimized, since both $I_{spin\text{-}boson}$ and $N_{av}(t)$ are saturated less than the page value [Figs. 4(e)–4(h)].

(iii) For increasing κ, the saturation value is further reduced. At the same time, for the nonergodic phase, this saturation value is less than its ergodic counterpart [Figs. 4(i)–4(p)].

(iv) For the higher-κ regime, the saturation value and the corresponding saturation time are independent of ω_d [Figs. 4(n) and 4(p)].

In summary, dissipation plays a constructive role in stabilizing the long-lived prethermal phase. In the next section, we also discuss the possible implications of our results for the rectification of an erroneous Floquet drive.

V. CONCLUSION

We have presented a brief analysis of the existing phase transitions in the ADM in the presence of dissipation. The QPT in this case is modified by anisotropy ($g_1 \neq g_2$) and finite dissipation ($\kappa > 0$). The ADM also shows the ENET, as the vicinity of $g_1 = 0$ or $g_2 = 0$ shows the notion of nonergodic phase, and the remaining part shows the ergodic behavior. Our result suggests that, in the presence of weak dissipation, the system continues to exhibit nonergodic behavior in the vicinity of $g_1 = 0$ or $g_2 = 0$. We supported our claim with the study of the Liouvillian $\hat{\hat{\mathcal{L}}}$ of the atom plus cavity. The Liouvillian gap Δ shows two different scalings of ergodic and nonergodic phases for changing atom numbers. Similarly, the average participation ratio of the eigenvectors explicitly shows the notion of the ENET.

We would like to emphasize that the ergodic-nonergodic behavior in open quantum systems remains an active area of research, and a comprehensive understanding is still lacking. A commonly used and intuitive way to characterize the ergodic-nonergodic transition in dissipative systems is based on symmetry and Liouvillian structure: A system is considered nonergodic if it exhibits multiple steady states or if the steady state is unique but associated with a diverging relaxation timescale. In this work, however, we addressed the problem from a complementary perspective. We began with an isolated quantum many-body system where the parameter regime exhibiting the ENET is already well established. Our goal was to examine how these features are affected when a weak dissipation is introduced. In particular, we investigated whether signatures of the transition persist within the same parameter regime or whether they are modified, quantitatively or qualitatively, by the presence of even small coupling to the environment. Our intuition suggests that one should not expect an abrupt change in behavior upon introducing weak dissipation. Indeed, several works in the literature support this point of view [72,74]. In this sense, our contribution is to extend such an analysis by explicitly incorporating the structure of the Liouvillian, thereby providing a complementary perspective on how these features manifest in the dynamics of dissipative many-body systems. Additionally, we showed that the QPT is associated with the eigenstate corresponding to the eigenvalue of zero real part of the Liouvillian, while the ENET is connected to its decaying modes (Fig. 3). These phenomena exhibit a one-to-one correspondence with their closed-system counterparts, i.e., the QPT is a ground-state phenomenon, whereas the ENET is associated with the middle of the excited-state spectrum [25]. We note that the mean-field studies are typically confined to steady-state properties, and hence a beyond-mean-field analysis (i.e., cumulant-expansion scheme) is required to understand integrability breaking in dissipative many-body systems [76–78].

We have also provided an intuitive physical mechanism for such scaling behavior of the Liouvillian gap. The key difference arises from the nature of the information spread and the relaxation in the two phases. Even though the Liouvillian always has a unique steady state (a single zero eigenvalue), the approach to that steady state is governed by the rest of the spectrum, which can behave very differently across regimes. In particular, different dynamical phases can exhibit distinct finite-size scaling of the Liouvillian gap without any change in the steady-state uniqueness. In an ergodic regime, relaxation involves exploration of an extensive portion of the configuration space, so the slowest nontrivial decay mode becomes increasingly long lived as the system size grows. In contrast, in a nonergodic or constrained regime, relaxation is governed by local or effectively finite-dimensional subspaces of the full Hilbert and configuration space [29]. The slowest decay channel then remains set by local processes and does not become parametrically slower with system size, resulting in a finite asymptotic gap, as shown in Fig. 1. However, a more detailed analysis is required for a rigorous justification at the thermodynamic limit.

Finally, we considered the driven ADM, where the periodic drive leads the system to the prethermal phase. A modification of the periodic Floquet drive (e.g., quasiperiodic drive) further introduces the heating process of the prethermal state. We found that the presence of dissipation is beneficial in this case. It is known that a reservoir engineering protocol can be used for the ground state or targeted state preparation, as the unwanted excitation can be released through the leaking cavity to the environment. Motivated by this fact, we aimed to investigate a similar situation here. Our result indicates that dissipation halts the excessive heating for the quasiperiodic case [Figs. 4(e)–4(p)]. For the experimental realization, we need to design a driving protocol that interpolates between the two types of drives: $f(t) = a_1 \cos(\omega_d t) + a_2 \cos(\alpha \omega_d t)$. Here α is an irrational number. In the case of nuclear magnetic resonance, such a quasiperiodic drive is already implemented by providing two periodic delta kicks in the y direction, with $\alpha = (\sqrt{5}+1)/2$ to observe discrete time quasicrystals [79].

We also present possible future directions for our research. An extension of our analysis to the thermal phase transition and excited-state quantum phase transition that incorporates dissipation is required. Similarly, the study of boundary or discrete time crystals, a π spin glass in the dissipative ADM under periodic driving, and the emergence of superradiant emission would be of interest for understanding dynamical phases [80–83]. Another interesting avenue for future research is to investigate the dynamics of the ADM in an accelerated reference frame, where the Unruh effect may be significantly modified by the presence of anisotropy. Such a study could provide new insight into the interplay between nonequilibrium quantum criticality and relativistic quantum effects [84]. Furthermore, the rapidly increasing dimensionality of the Liouvillian poses a challenge for simulating large atomic ensembles; addressing this issue will require the development of advanced numerical techniques in future work.

ACKNOWLEDGMENTS

We sincerely thank Auditya Sharma and Devendra Singh Bhakuni for fruitful discussions and constructive comments. We are especially grateful to the anonymous referees for their extensive critical and constructive feedback that helped strengthen this paper. We are also grateful to the High-Performance Computing (HPC) facility at IISER Bhopal. P.D. acknowledges IISERB for providing the Ph.D. fellowship that supported the initial phase of this project. P.D. also acknowledges support from the European Research Council (ERC) through a postdoctoral fellowship (Project No. N1-0273) in Slovenia. S.S. thanks the University Grants Commission (UGC) for providing a Ph.D. fellowship (Student ID: MAY 2018528071) in India, which supported the initial phase of this research. S.S. also acknowledges research support and funding from BERLIN QUANTUM, an initiative endowed by the Innovation Promotion Fund of the city of Berlin and the Deutsche Forschungsgemeinschaft (DFG, German Research Foundation) via the Research Unit FOR 5688 (Project No. 521530974). We also thank ICTS-TIFR Bangalore, India for hosting the program "Stability of Quantum Matter in and out of Equilibrium at Various Scales", (Program No. ICTS/SQMVS2024/01), where this work and the associated discussions were initiated.

DATA AVAILABILITY

The data that support the findings of this article are not publicly available upon publication because it is not technically feasible and/or the cost of preparing, depositing, and hosting the data would be prohibitive within the terms of this research project. The data are available from the authors upon reasonable request.

APPENDIX A: EIGENVALUE PROPERTIES

We provide a brief review of the distribution function of the eigenvalues and level-spacing ratios of a many-body quantum system, which motivates us to study the nature of such a function for this model. Based on the eigenvalue distribution of a Hermitian system, it can be broadly classified into two categories: (i) regular, integrable, or nonergodic and (ii) chaotic or ergodic. Berry and Tabor hypothesized [85] that, for integrable systems, the levels are uncorrelated, and hence the level-spacing distribution follows the one-dimensional Poisson distribution. However, for correlated spectrum, the famous Wigner conjecture [30] is a powerful tool to investigate the spacing distribution. Bohigas *et al*. hypothesized [86] that chaotic systems would follow statistical behavior described by random matrix theory appropriate to their symmetry classes. Following Bohigas *et al*., Grobe *et al*. [54] expanded the above spectral contrast between integrability and chaos for Markovian open quantum systems. They found that in the integrable limit, the nearest-neighbor spacing distribution of radial distance s for the complex eigenvalues of Liouvillian agrees with the two-dimensional (2D) Poisson distribution. Such a distribution is the same as Wigner's conjecture for the spacing distribution in the Gaussian orthogonal ensemble. In contrast, for a fully chaotic limit, the spacing distribution agrees with the Ginibre ensemble [53–57].

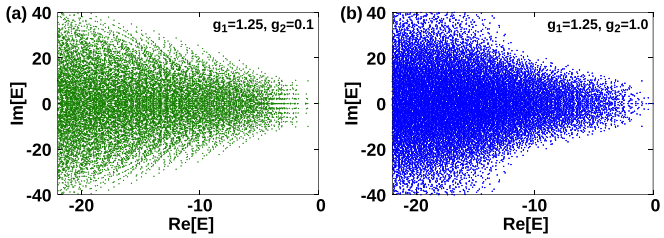


FIG. 5. Scatter plot of the complex spectrum of the Liouvillian $\hat{\hat{\mathcal{L}}}$ of the dissipative anisotropic Dicke model, with $N = 10$, $n_{\max} = 26$, and $\omega = \omega_0 = \kappa = 1$, for (a) a point in the nonergodic phase ($g_1 = 1.25$, $g_2 = 0.1$) and (b) a point in the ergodic phase ($g_1 = 1.25$, $g_2 = 1.0$).

Here we study the eigenvalue properties of the Liouvillian $\hat{\hat{\mathcal{L}}}$. Since complex eigenvalues are involved, we consider generalized notions of the level-spacing distribution and the consecutive level-spacing ratio [72]. By analyzing these quantities as a function of the coupling parameters, we try to sketch the phase diagram, which carries information on the nonergodic to ergodic phase transition in the dissipative ADM. The eigenvalues of $\hat{\hat{\mathcal{L}}}$ lie in the nonpositive plane, which prevents the divergence of Eq. (2). The nonreal eigenvalues possess complex conjugates, demonstrating the Hermiticity of the density matrix. The zero eigenvalue of $\hat{\hat{\mathcal{L}}}$ corresponds to a steady state. The real part of the complex eigenvalues corresponds to the loss or decay of the initial density matrix [43].

In Fig. 5 we show the scatter plot of the complex spectrum of the Liouvillian $\hat{\hat{\mathcal{L}}}$ for two different set of (g_1, g_2) pairs, $g_1 = 1.25$ and $g_2 = 0.1$ [Fig. 5(a)] and 5(b) $g_1 = 1.25$ and $g_2 = 1.0$ [Fig. 5(b)], corresponding to the nonergodic and ergodic regimes, respectively. The plots clearly show the different natures of the spectrum in the regular and chaotic regimes, respectively. For a clearer understanding of the two different phases, one should study the level-spacing statistics. Additionally, we would like to discuss briefly how to calculate the level-spacing distribution for a non-Hermitian system.

We first carry out an unfolding of the spectrum to remove the system-specific aspects of the level-spacing statistics. The complex level-spacing distribution $P(s)$ is then produced by using the unfolded spectrum to create a histogram of the Euclidean distance s between nearest-neighbor eigenvalues in the complex plane. For the unfolding process, we mainly follow Refs. [56,57,87].

The nearest-neighbor (NN) Euclidean distance of each eigenvalue of the Liouvillian is given by $s_i \equiv |E_i - E_i^{\mathrm{NN}}|$. After rescaling, the analytical expression is given by

$$s_i \to s_i' = s_i \frac{\sqrt{\rho_{\mathrm{av}}(E_i)}}{\bar{s}}. \tag{A1}$$

Here $\rho_{\mathrm{av}}(E_i)$ is the local average density, which can be approximated as

$$\rho_{\mathrm{av}}(E_i) = \frac{1}{2\pi\sigma^2 N} \sum_{i=1}^{N} \exp\left(-\frac{|E - E_i|^2}{2\sigma^2}\right). \tag{A2}$$

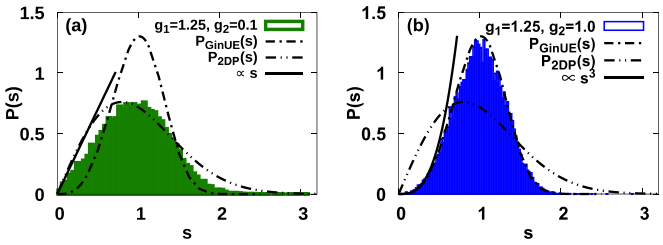


FIG. 6. Level-spacing distribution of the complex spectrum of the Liouvillian $\hat{\hat{\mathcal{L}}}$ in (a) the nonergodic phase with $g_1 = 1.25$, $g_2 = 0.1$ and (b) the ergodic phase with $g_1 = 1.25$, $g_2 = 0.1$. For (a), we find excellent agreement with the two-dimensional Poisson distribution ($P_{2DP}(s)$) [Eq. (A3)], whereas for (b), the level-spacing distribution is in excellent agreement with the Ginibre unitary ensemble (GinUE) random-matrix prediction ($P_{GinUE}(s)$) [Eq. (A4)]. The other parameters are: $\omega = \omega_0 = 1$, $\kappa = 1$.

Following Refs. [56,57,87], we choose $\sigma = 4.5\bar{s}$, where $\bar{s} = \frac{1}{N}\sum_{i=1}^{N} s_i$. In Eq. (A1) $\bar{s}$ is chosen such that $\frac{1}{N}\sum_{i=1}^{N} s'_i = 1$. Finally, we will study the level statistics of the NN distance s'_i.

The analytical form of the 2D Poisson distribution, which corresponds to the spacing distribution for independent complex random values, is given by

$$P_{2DP}(s) = \frac{\pi}{2} s \exp\left(-\frac{\pi s^2}{4}\right). \tag{A3}$$

In contrast, for the fully chaotic (or ergodic) limit, the spacing distribution agrees with the corresponding distribution of the Ginibre ensemble of complex Gaussian non-Hermitian random matrices, given by

$$P_{GinUE}(s) = \bar{s}\bar{P}_{GinUE}(\bar{s}s), \tag{A4}$$

with

$$\bar{P}_{GinUE}(s) = \sum_{j=1}^{\infty} \frac{2s^{2j+1}\exp(-s^2)}{\Gamma(1+j,s^2)} \prod_{k=1}^{\infty} \frac{\Gamma(1+k,s^2)}{k!} \tag{A5}$$

and $\bar{s} = \int_0^\infty s\bar{P}_{GinUE}(s)\,ds$, where $\Gamma(1+k,s^2) = \int_{s^2}^\infty t^k e^{-t} dt$ is the incomplete Gamma function.

We study the level-spacing statistics separately for these two pair points in different phases (see Fig. 6). Figure 6

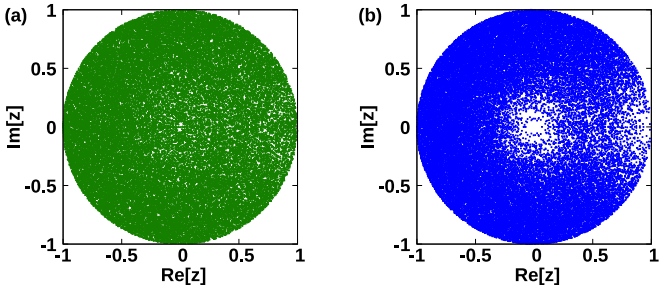


FIG. 7. Scatter plot of the complex level-spacing ratio z introduced in Eq. (A6) for $N = 10$ and $n_{max} = 26$, for (a) a point in the nonergodic phase ($g_1 = 1.25$, $g_2 = 0.1$), which shows the isotropic behavior, and (b) a point in the ergodic phase ($g_1 = 1.25$, $g_2 = 1.0$), which is not isotropic. The other parameters are $\omega = \omega_0 = 1$ and $\kappa = 1$.

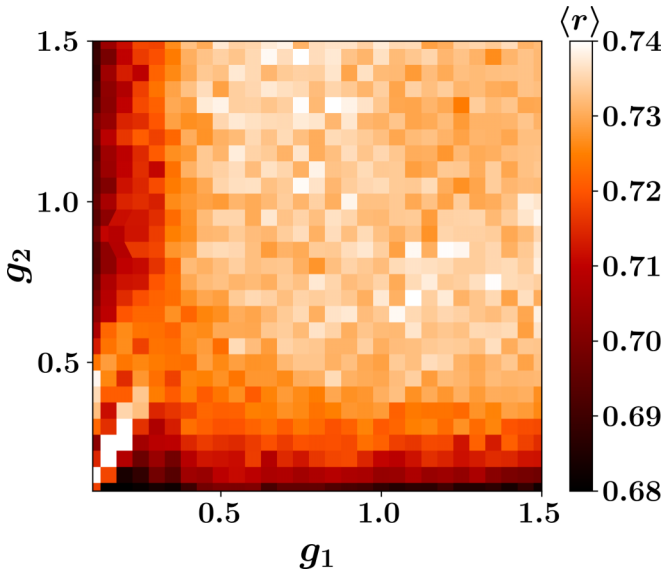


FIG. 8. Average level-spacing ratio $\langle r \rangle$ of the dissipative anisotropic Dicke model, showing a transition from the nonergodic phase (where the system follow the 2D Poisson statics and $\langle r \rangle \approx 0.69$) to the ergodic phase (where the system behaves as the Ginibre ensemble and $\langle r \rangle \approx 0.74$). The other parameters are $N = 8$, $n_{max} = 20$, $\omega = \omega_0 = 1$, and $\kappa = 1$.

displays the striking agreement between the distributions calculated from the spectrum of $\hat{\hat{\mathcal{L}}}$ and the 2D Poisson distribution in the integrable, regular, or nonergodic regime and the GinUE forecast in the chaotic or ergodic regime, respectively. In the ergodic phase $P(s) \approx s^3$, which indicates the chaotic behavior of the complex eigenvalues as they repel each other,

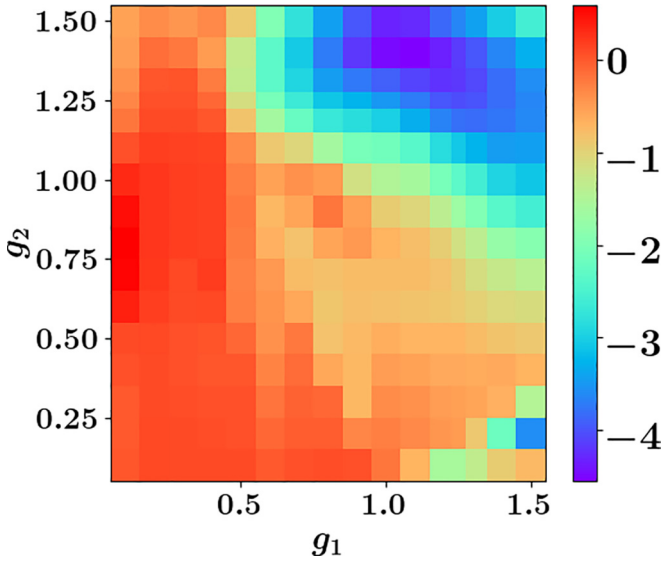


FIG. 9. Exponent z (extracted from the scaling of the Liouvillian gap Δ as a function of atom number) as a function of g_1 and g_2 for $\kappa = 0.1$ and $n_{max} = 26$. Here the atom number N is changing from 4 to 10. For varying g_1 and g_2, the system shows a response that is similar to the ENET. For example, in the vicinity of $g_1 = 0$ and $g_2 = 0$ (nonergodic phase), the value of z (dark orange portion) is different from the remaining part (ergodic phase).

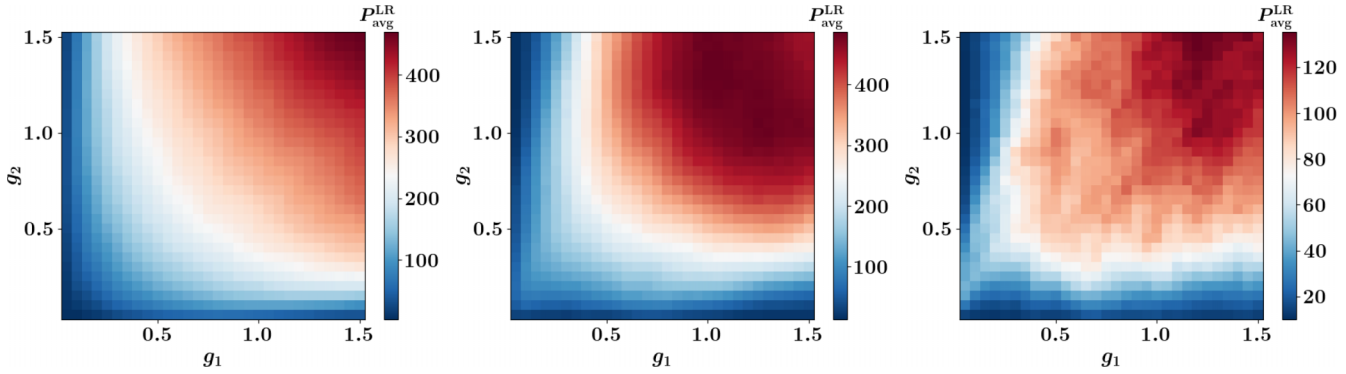


FIG. 10. Average participation ratio $P_{\text{av}}^{\text{LR}}$, using a biorthonormal basis considering both left and right eigenvectors of the Liouvillian for the dissipative ADM as a function of the rotating and counterrotating coupling parameters g_1 and g_2, with $N = 4$, $n_{\text{max}} = 10$, $\omega_0 = \omega = 1$, and (a) $\kappa = 1.0$, (b) $\kappa = 0.1$, and (c) $\kappa = 0.01$.

and this is consistent with Ginibre distribution in Eq. (A4). On the other hand, in the nonergodic phase, we have $P(s) \approx s$, indicating the integrable nature of this regime and consistent with 2D Poisson distribution in the complex plane.

Consecutive level-spacing ratio

The complex level-spacing ratio [72,88] can be defined as

$$z_i = r_i e^{i\theta_i} = \frac{E_i^{\text{NN}} - E_i}{E_i^{\text{NNN}} - E_i} \tag{A6}$$

for the NN and next-nearest-neighbor eigenvalues. It captures the information about the next closest neighbor that is overlooked in the level-spacing statistics. The advantage of the calculation is that we do not require the unfolding procedure. In Fig. 7 we show the scatter plot of z in the nonergodic ($g_1 = 1.25$ and $g_2 = 0.1$) and ergodic phases ($g_1 = 1.25$ and $g_2 = 1.0$) separately. For the nonergodic case, the scatter plot is symmetric and isotropic, whereas for the ergodic case, it is anisotropic, which is another signature of the connection to random matrix theory [88]. In Fig. 8 we show the absolute value of the average level-spacing ratio for this model. The figure shows a nonergodic phase to ergodic phase transition similar to the closed ADM [25]. Here, in the nonergodic phase, $\langle r \rangle \approx 0.69$ (dark color), which is equivalent to the system following the 2D Poisson distribution, whereas in the ergodic phase, $\langle r \rangle \approx 0.74$ (light color), which corresponds to the Ginibre unitary ensemble.

APPENDIX B: DEPENDENCE OF THE EXPONENT z ON VARYING g_1 AND g_2

In Fig. 9 we provide a contour plot of the exponent z by varying g_1 and g_2 for $\kappa = 0.1$. Our results successfully capture the key features of the system, even though the extreme point ($g_1 = g_2$), which occurs farthest from the integrability, is not yet clearly visible. Nevertheless, the dependence of z on g_1 and g_2 shows qualitative similarities to the ENET. To achieve a clearer understanding, simulations with a larger number of atoms and a higher bosonic cutoff will be required.

APPENDIX C: AVERAGE PARTICIPATION RATIO FOR DIFFERENT κ

Here we provide the contour plots of $P_{\text{av}}^{\text{LR}}$ for different κ by varying g_1 and g_2 in Fig. 10. We observe that the study of $P_{\text{av}}^{\text{LR}}$ successfully captures the ENET, and for changing κ, the qualitative features remain unchanged.

[1] C. Cohen-Tannoudji, J. Dupont-Roc, and G. Grynberg, *Atom-Photon Interactions: Basic Processes and Applications* (Wiley, New York, 1998).

[2] J. Léonard, A. Morales, P. Zupancic, T. Donner, and T. Esslinger, Monitoring and manipulating Higgs and Goldstone modes in a supersolid quantum gas, Science **358**, 1415 (2017).

[3] R. Gutzler, M. Garg, C. R. Ast, K. Kuhnke, and K. Kern, Light–matter interaction at atomic scales, Nat. Rev. Phys. **3**, 441 (2021).

[4] D. E. Chang, J. S. Douglas, A. González-Tudela, C.-L. Hung, and H. J. Kimble, *Colloquium*: Quantum matter built from nanoscopic lattices of atoms and photons, Rev. Mod. Phys. **90**, 031002 (2018).

[5] H. Walther, B. T. H. Varcoe, B.-G. Englert, and T. Becker, Cavity quantum electrodynamics, Rep. Prog. Phys. **69**, 1325 (2006).

[6] A. Reiserer and G. Rempe, Cavity-based quantum networks with single atoms and optical photons, Rev. Mod. Phys. **87**, 1379 (2015).

[7] V. D. Vaidya, Y. Guo, R. M. Kroeze, K. E. Ballantine, A. J. Kollár, J. Keeling, and B. L. Lev, Tunable-range, photon-mediated atomic interactions in multimode cavity QED, Phys. Rev. X **8**, 011002 (2018).

[8] F. Dimer, B. Estienne, A. S. Parkins, and H. J. Carmichael, Proposed realization of the Dicke-model quantum phase transition in an optical cavity QED system, Phys. Rev. A **75**, 013804 (2007).

[9] B. M. Garraway, The Dicke model in quantum optics: Dicke model revisited, Philos. Trans. R. Soc. A **369**, 1137 (1939).

[10] P. Kirton, M. M. Roses, J. Keeling, and E. G. Dalla Torre, Introduction to the Dicke model: From equilibrium to nonequilibrium, and vice versa, Adv. Quantum Technol. **2**, 1800043 (2019).

[11] D. Villaseñor, S. Pilatowsky-Cameo, J. Chávez-Carlos, M. A. Bastarrachea-Magnani, S. Lerma-Hernández, L. F. Santos, and J. G. Hirsch, Classical and quantum properties of the spin-boson Dicke model: Chaos, localization, and scarring, arXiv:2405.20381.

[12] R. H Dicke, Coherence in spontaneous radiation processes, Phys. Rev. **93**, 99 (1954).

[13] N. Lambert, C. Emary, and T. Brandes, Entanglement and the phase transition in single-mode superradiance, Phys. Rev. Lett. **92**, 073602 (2004).

[14] C. Emary and T. Brandes, Chaos and the quantum phase transition in the Dicke model, Phys. Rev. E **67**, 066203 (2003).

[15] C. Emary and T. Brandes, Quantum chaos triggered by precursors of a quantum phase transition: The Dicke model, Phys. Rev. Lett. **90**, 044101 (2003).

[16] J. Chávez-Carlos, M. A. Bastarrachea-Magnani, S. Lerma-Hernández, and J. G. Hirsch, Classical chaos in atom-field systems, Phys. Rev. E **94**, 022209 (2016).

[17] P. Kirton and J. Keeling, Superradiant and lasing states in driven-dissipative Dicke models, New J. Phys. **20**, 015009 (2018).

[18] P. Das and A. Sharma, Revisiting the phase transitions of the Dicke model, Phys. Rev. A **105**, 033716 (2022).

[19] P. Das, S. Wüster, and A. Sharma, Dicke model with disordered spin-boson couplings, Phys. Rev. A **109**, 013715 (2024).

[20] K. Baumann, C. Guerlin, F. Brennecke, and T. Esslinger, Dicke quantum phase transition with a superfluid gas in an optical cavity, Nature (London) **464**, 1301 (2010).

[21] R. Gutiérrez-Jáuregui and H. J. Carmichael, Dissipative quantum phase transitions of light in a generalized Jaynes-Cummings-Rabi model, Phys. Rev. A **98**, 023804 (2018).

[22] W. Buijsman, V. Gritsev, and R. Sprik, Nonergodicity in the anisotropic Dicke model, Phys. Rev. Lett. **118**, 080601 (2017).

[23] M. Kloc, P. Stránský, and P. Cejnar, Quantum phases and entanglement properties of an extended Dicke model, Ann. Phys. (N.Y.) **382**, 85 (2017).

[24] D. S. Shapiro, W. V. Pogosov, and Y. E. Lozovik, Universal fluctuations and squeezing in a generalized Dicke model near the superradiant phase transition, Phys. Rev. A **102**, 023703 (2020).

[25] P. Das, D. S. Bhakuni, and A. Sharma, Phase transitions of the anisotropic Dicke model, Phys. Rev. A **107**, 043706 (2023).

[26] J. Hu and S. Wan, Out-of-time-ordered correlation in anisotropic Dicke model, Commun. Theor. Phys. **73**, 125703 (2021).

[27] A. Polkovnikov, K. Sengupta, A. Silva, and M. Vengalattore, *Colloquium*: Nonequilibrium dynamics of closed interacting quantum systems, Rev. Mod. Phys. **83**, 863 (2011).

[28] T. Mori, T. N. Ikeda, E. Kaminishi, and M. Ueda, Thermalization and prethermalization in isolated quantum systems: A theoretical overview, J. Phys. B **51**, 112001 (2018).

[29] M. Serbyn, D. A. Abanin, and Z. Papić, Quantum many-body scars and weak breaking of ergodicity, Nat. Phys. **17**, 675 (2021).

[30] L. D'Alessio, Y. Kafri, A. Polkovnikov, and M. Rigol, From quantum chaos and eigenstate thermalization to statistical mechanics and thermodynamics, Adv. Phys. **65**, 239 (2016).

[31] F. Borgonovi, F. M. Izrailev, L. F. Santos, and V. G. Zelevinsky, Quantum chaos and thermalization in isolated systems of interacting particles, Phys. Rep. **626**, 1 (2016).

[32] M. J. Bhaseen, J. Mayoh, B. D. Simons, and J. Keeling, Dynamics of nonequilibrium Dicke models, Phys. Rev. A **85**, 013817 (2012).

[33] P. Kirton and J. Keeling, Suppressing and restoring the Dicke superradiance transition by dephasing and decay, Phys. Rev. Lett. **118**, 123602 (2017).

[34] H.-P. Breuer and F. Petruccione, *The Theory of Open Quantum Systems* (Oxford University Press, Oxford, 2002).

[35] T. Haga, M. Nakagawa, R. Hamazaki, and M. Ueda, Liouvillian skin effect: Slowing down of relaxation processes without gap closing, Phys. Rev. Lett. **127**, 070402 (2021).

[36] B. Zhou, X. Wang, and S. Chen, Exponential size scaling of the Liouvillian gap in boundary-dissipated systems with Anderson localization, Phys. Rev. B **106**, 064203 (2022).

[37] T. Prosen and I. Pižorn, Quantum phase transition in a far-from-equilibrium steady state of an *XY* spin chain, Phys. Rev. Lett. **101**, 105701 (2008).

[38] E. M. Kessler, G. Giedke, A. Imamoglu, S. F. Yelin, M. D. Lukin, and J. I. Cirac, Dissipative phase transition in a central spin system, Phys. Rev. A **86**, 012116 (2012).

[39] Z. Cai and T. Barthel, Algebraic versus exponential decoherence in dissipative many-particle systems, Phys. Rev. Lett. **111**, 150403 (2013).

[40] M. J. Kastoryano and J. Eisert, Rapid mixing implies exponential decay of correlations, J. Math. Phys. **54**, 102201 (2013).

[41] M. Žnidarič, Relaxation times of dissipative many-body quantum systems, Phys. Rev. E **92**, 042143 (2015).

[42] W. Casteels, R. Fazio, and C. Ciuti, Critical dynamical properties of a first-order dissipative phase transition, Phys. Rev. A **95**, 012128 (2017).

[43] F. Minganti, A. Biella, N. Bartolo, and C. Ciuti, Spectral theory of Liouvillians for dissipative phase transitions, Phys. Rev. A **98**, 042118 (2018).

[44] N. Shibata and H. Katsura, Dissipative spin chain as a non-Hermitian Kitaev ladder, Phys. Rev. B **99**, 174303 (2019).

[45] N. Shibata and H. Katsura, Dissipative quantum Ising chain as a non-Hermitian Ashkin-Teller model, Phys. Rev. B **99**, 224432 (2019).

[46] N. Shibata and H. Katsura, Quantum Ising chain with boundary dephasing, Prog. Theor. Exp. Phys. **2020**, 12A108 (2020).

[47] T. Mori and T. Shirai, Resolving a discrepancy between Liouvillian gap and relaxation time in boundary-dissipated quantum many-body systems, Phys. Rev. Lett. **125**, 230604 (2020).

[48] T. Mori and T. Shirai, Symmetrized Liouvillian gap in Markovian open quantum systems, Phys. Rev. Lett. **130**, 230404 (2023).

[49] T. Shirai and T. Mori, Accelerated decay due to operator spreading in bulk-dissipated quantum systems, Phys. Rev. Lett. **133**, 040201 (2024).

[50] T. Mori, Liouvillian-gap analysis of open quantum many-body systems in the weak dissipation limit, Phys. Rev. B **109**, 064311 (2024).

[51] G. T. Landi, D. Poletti, and G. Schaller, Nonequilibrium boundary-driven quantum systems: Models, methods, and properties, Rev. Mod. Phys. **94**, 045006 (2022).

[52] D. Yuan, H.-R. Wang, Z. Wang, and D.-L. Deng, Solving the Liouvillian gap with artificial neural networks, Phys. Rev. Lett. **126**, 160401 (2021).

[53] J. Ginibre, Statistical ensembles of complex, quaternion, and real matrices, J. Math. Phys. **6**, 440 (1965).

[54] R. Grobe, F. Haake, and H. Sommers, Quantum distinction of regular and chaotic dissipative motion, Phys. Rev. Lett. **61**, 1899 (1988).

[55] H. Markum, R. Pullirsch, and T. Wettig, Non-Hermitian random matrix theory and lattice QCD with chemical potential, Phys. Rev. Lett. **83**, 484 (1999).

[56] F. Haake, Quantum signatures of chaos, in *Quantum Coherence in Mesoscopic Systems*, edited by B. Kramer, NATO ASI Series (Springer, Boston, MA, 1991), Vol. 254, pp. 583–595.

[57] R. Hamazaki, K. Kawabata, N. Kura, and M. Ueda, Universality classes of non-Hermitian random matrices, Phys. Rev. Res. **2**, 023286 (2020).

[58] A. Eckardt, *Colloquium*: Atomic quantum gases in periodically driven optical lattices, Rev. Mod. Phys. **89**, 011004 (2017).

[59] D. A. Abanin, E. Altman, I. Bloch, and M. Serbyn, *Colloquium*: Many-body localization, thermalization, and entanglement, Rev. Mod. Phys. **91**, 021001 (2019).

[60] R. Nandkishore and D. A. Huse, Many-body localization and thermalization in quantum statistical mechanics, Annu. Rev. Condens. Matter Phys. **6**, 15 (2015).

[61] D. A. Abanin, W. De Roeck, and F. Huveneers, Exponentially slow heating in periodically driven many-body systems, Phys. Rev. Lett. **115**, 256803 (2015).

[62] W. Beatrez, O. Janes, A. Akkiraju, A. Pillai, A. Oddo, P. Reshetikhin, E. Druga, M. McAllister, M. Elo, B. Gilbert, D. Suter, and A. Ajoy, Floquet prethermalization with lifetime exceeding 90 s in a bulk hyperpolarized solid, Phys. Rev. Lett. **127**, 170603 (2021).

[63] S. Saha and R. Bhattacharyya, Cascaded dynamics of a periodically driven dissipative dipolar system, Phys. Rev. A **107**, 022206 (2023).

[64] P. Das, D. S. Bhakuni, L. F. Santos, and A. Sharma, Periodically and quasiperiodically driven anisotropic Dicke model, Phys. Rev. A **108**, 063716 (2023).

[65] C. Fleckenstein and M. Bukov, Prethermalization and thermalization in periodically driven many-body systems away from the high-frequency limit, Phys. Rev. B **103**, L140302 (2021).

[66] S. Nandy, A. Sen, and D. Sen, Aperiodically driven integrable systems and their emergent steady states, Phys. Rev. X **7**, 031034 (2017).

[67] B. Mukherjee, A. Sen, D. Sen, and K. Sengupta, Restoring coherence via aperiodic drives in a many-body quantum system, Phys. Rev. B **102**, 014301 (2020).

[68] H. Zhao, F. Mintert, R. Moessner, and J. Knolle, Random multipolar driving: Tunably slow heating through spectral engineering, Phys. Rev. Lett. **126**, 040601 (2021).

[69] H. Zhao, F. Mintert, J. Knolle, and R. Moessner, Localization persisting under aperiodic driving, Phys. Rev. B **105**, L220202 (2022).

[70] V. Tiwari, D. S. Bhakuni, and A. Sharma, Dynamical localization and slow dynamics in quasiperiodically driven quantum systems, Phys. Rev. B **109**, L161104 (2024).

[71] V. Tiwari, D. S. Bhakuni, and A. Sharma, Periodically and aperiodically Thue-Morse driven long-range systems: From dynamical localization to slow dynamics, Phys. Rev. B **111**, 205109 (2025).

[72] M. Prasad, H. K. Yadalam, C. Aron, and M. Kulkarni, Dissipative quantum dynamics, phase transitions, and non-Hermitian random matrices, Phys. Rev. A **105**, L050201 (2022).

[73] S. Saha and R. Bhattacharyya, Prethermalization in an open quantum system coupled to a spatially correlated bosonic bath, J. Stat. Mech. (2024) 023103.

[74] D. Villaseñor, L. F. Santos, and P. Barberis-Blostein, Breakdown of the quantum distinction of regular and chaotic classical dynamics in dissipative systems, Phys. Rev. Lett. **133**, 240404 (2024).

[75] K. Suthar, Y.-C. Wang, Y.-P. Huang, H. H. Jen, and J.-S. You, Non-Hermitian many-body localization with open boundaries, Phys. Rev. B **106**, 064208 (2022).

[76] S. Krämer and H. Ritsch, Generalized mean-field approach to simulate the dynamics of large open spin ensembles with long range interactions, Eur. Phys. J. D **69**, 282 (2015).

[77] R. Holzinger, O. Rubies-Bigorda, S. F. Yelin, and H. Ritsch, Symmetry-based efficient simulation of higher-order coherences in quantum many-body superradiance, Phys. Rev. Res. **7**, 033203 (2025).

[78] J. Kerber, H. Ritsch, and L. Ostermann, The cumulants expansion approach: The good, the bad and the ugly, arXiv:2511.20115.

[79] G. He, B. Ye, R. Gong, C. Yao, Z. Liu, K. W. Murch, N. Y. Yao, and C. Zu, Experimental realization of discrete time quasicrystals, Phys. Rev. X **15**, 011055 (2025).

[80] S. B. Jäger, J. M. Giesen, I. Schneider, and S. Eggert, Dissipative Dicke time crystals: An atom's point of view, Phys. Rev. A **110**, L010202 (2024).

[81] S. Saha and R. Bhattacharyya, Prethermal discrete time crystal in driven-dissipative dipolar systems, Phys. Rev. A **109**, 012208 (2024).

[82] G. Das, S. Saha, and R. Bhattacharyya, Environment-assisted discrete time crystals in noninteracting quantum systems, Phys. Rev. A **113**, 042216 (2026).

[83] S. Saha, Y. Ibrahim, and R. Bhattacharyya, Emergence of superradiance in dissipative dipolar-coupled spin systems, J. Phys. A: Math. Theor. **58**, 035302 (2025).

[84] S. Saha, C. Singha, P. Das, and A. Chatterjee, Emergence of Unruh prethermalization for uniformly accelerating many-atom system, Phys. Rev. D **113**, 065011 (2026).

[85] M. V. Berry and M. Tabor, Level clustering in the regular spectrum, Proc. R. Soc. London A **356**, 375 (1977).

[86] O. Bohigas, M. J. Giannoni, and C. Schmit, Characterization of chaotic quantum spectra and universality of level fluctuation laws, Phys. Rev. Lett. **52**, 1 (1984).

[87] G. Akemann, M. Kieburg, A. Mielke, and T. Prosen, Universal signature from integrability to chaos in dissipative open quantum systems, Phys. Rev. Lett. **123**, 254101 (2019).

[88] L. Sá, P. Ribeiro, and T. Prosen, Complex spacing ratios: A signature of dissipative quantum chaos, Phys. Rev. X **10**, 021019 (2020).